Eur. Phys. J. B **33**, 183–191 (2003)
DOI: 10.1140/epjb/e2003-00155-x

THE EUROPEAN PHYSICAL JOURNAL B

Covalent magnetism in the RFe_6Ge_6 series

T. Mazet[1,a], J. Tobola[1,2], and B. Malaman[1]

[1] Laboratoire de Chimie du Solide Minéral, Université Henri Poincaré-Nancy I[b], BP 239, 54506 Vandoeuvre-les-Nancy Cedex, France
[2] Faculty of Physics and Nuclear Techniques, University of Mining and Metallurgy, Al. Mickiewicza 30, 30-059 Crakow, Poland

Received 20 December 2002
Published online 4 June 2003 –

Abstract. The electronic structure of the RFe_6Ge_6 compounds (R = Sc, Lu, Ti, Zr, Hf and Nb) of $HfFe_6Ge_6$-type structure has been studied using the muffin-tin Korringa-Kohn-Rostoker method in a non-relativistic approach. The chemical bonding is analyzed based on the *l*-decomposed site projected densities of states. Spin-dependent changes in the R *nd*- Fe 3*d* covalent bond are shown to be responsible for the experimentally observed rise in the Fe moment and hyperfine field upon increasing the R valency. The limited quantitative agreement between theoretical and experimental values is interpreted as being due to a non-negligible orbital moment and to a significant asphericity in the spin density at the iron site. The theoretical results also forecast a strong increase of the Ge(2e) *transferred* hyperfine field with the R valency.

PACS. 71.20.Lp Intermetallic compounds – 75.50.Ee Antiferromagnetics

1 Introduction

Most of the layered RFe_6Ge_6 compounds involving a transition element R (R = Sc, Lu, Ti, Zr, Hf and Nb) crystallize in the $HfFe_6Ge_6$-type structure (P6/mmm) [1–4]. These compounds may be seen as resulting from the ordered insertion of the R atom within half of Fe-Ge-Fe slabs of the CoSn-type [5] FeGe binary parent compound (Fig. 1). This insertion leads to a shift of the axial neighbor Ge atoms outside of the (001) Fe layers and, as shown in Figure 2, to a shortening of the interplanar Fe-Fe distance ($d_{\mathrm{Fe-Fe}} = c_{\mathrm{FeGe}} \approx \frac{1}{2} c_{R\mathrm{Fe_6Ge_6}}$). Both structures show close structural relationships with the $CaCu_5$-type [5] of the well-known RCo_5 compounds (Fig. 1).

The magnetic properties of RFe_6Ge_6 have been the subject to extensive experimental investigations using magnetic measurements, neutron powder diffraction and ^{57}Fe Mössbauer spectroscopy experiments [2–4,6,7]. The Fe sublattice orders magnetically with Néel points well above room temperature, the magnetic structure being built upon ferromagnetic easy-axis (001) Fe planes antiferromagnetically stacked (+ − + −) along the *c*-axis (Fig. 1). A rise in the iron magnetic moment (from m_{Fe} = 1.45 μ_B for R = Lu up to m_{Fe} = 2.05 μ_B for R = Nb), in the iron hyperfine field (from H_{Fe} = 16.1 T up to H_{Fe} = 24.0 T) and in the ordering temperature (from T_N = 464 K up to T_N = 561 K) are observed upon increasing the R valency (Fig. 3) [4,6,7]. Note that these quantities are lower for a 5*d* R element than for an isovalent 3*d* or 4*d* one. At low temperatures, magnetic measurements [7] and ^{57}Fe Mössbauer experiments [4,6] reveal the occurrence of slight deviations from this simple uniaxial antiferromagnetic behavior, undetected in the powder neutron diffraction patterns. These deviations consist in a small spread in the iron moment direction around the *c*-axis. Due to the local orthorhombic symmetry at the iron site, this allows the observation of anisotropic contributions (of orbital and/or dipolar origin) to the total iron hyperfine field. Binary FeGe (T_N = 400 K) presents a quite similar magnetic behavior [8,9] and it was found from single crystal neutron diffraction [10] that its low temperature magnetic structure is a *c*-axis double cone with a cone half-angle of 14° at 4.2 K (m_{Fe} = 1.60 μ_B).

Knowledge of the electronic structure of the RFe_6Ge_6 series is expected to give a better understanding of these experimental results. In this paper, we have investigated the electronic structure of RFe_6Ge_6 (R = Sc, Lu, Ti, Zr, Hf and Nb) and FeGe, using the nonrelativistic muffin-tin Korringa-Kohn-Rostoker (KKR) method in the local density approximation (LDA). The results emphasize the role of the spin-dependency of the hybridization in magnetically ordered materials. This mechanism was termed covalent magnetism by Williams *et al.* [14] when restricted to covalent interaction between *d* states, but similar

[a] e-mail: Thomas.Mazet@lcsm.uhp-nancy.fr
[b] Associé au CNRS (UMR 7555)

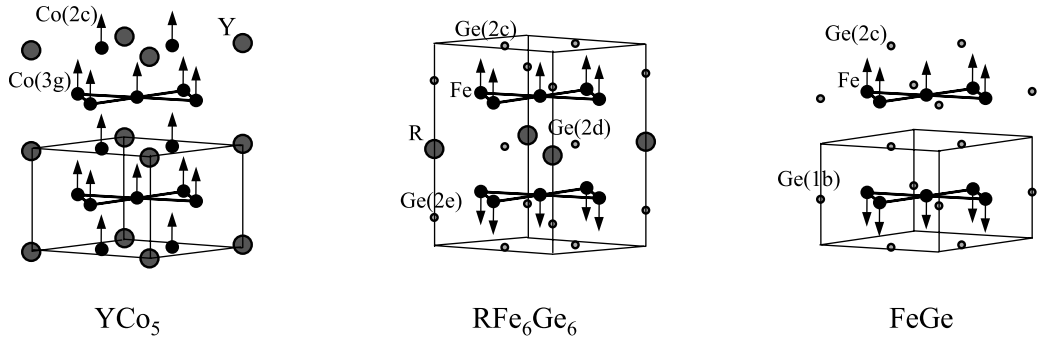

Fig. 1. Crystal and magnetic structures of YCo_5, RFe_6Ge_6 and FeGe.

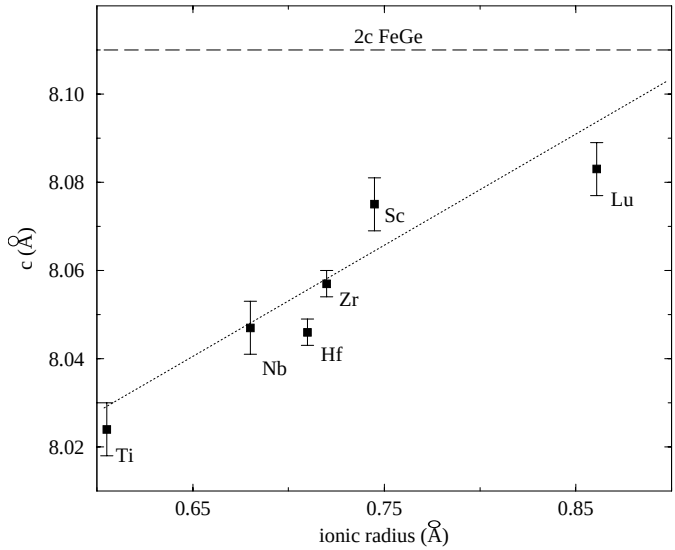

Fig. 2. Variation of the c parameter of the RFe_6Ge_6 cell as a function of the ionic radius of the R element (R = Sc, Lu, Ti, Zr, Hf and Nb) [4,6]. The dashed horizontal line locates the value corresponding to two times the FeGe c parameter [5]. The dotted line is a guide for the eye.

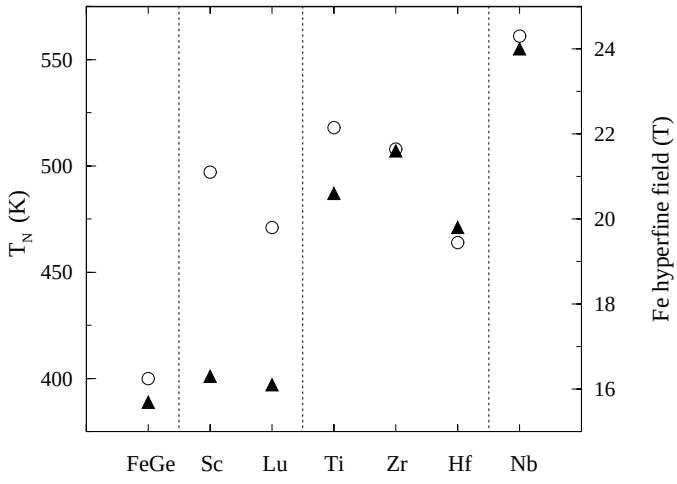

Fig. 3. Variation of the Néel temperature (open circles, left scale) and of the experimental Fe hyperfine field (full triangles, right scale) within the RFe_6Ge_6 series [4,6,7]. Also shown are data concerning FeGe [8].

arguments are still valid when dealing with *sd* hybridization [15]. Such spin-dependent hybridization is invoked, for instance, to account for the systematic negative sign of the exchange coupling between rare-earth and transition element spin moments in intermetallics [16,17] or to explain the *transferred* hyperfine fields on the nucleus of nominally diamagnetic atoms [18–20]. Furthermore, this study usefully completes previous theoretical works carried out on the isotypic RMn_6Sn_6 [11], RMn_6Ge_6 [12] and RFe_6Sn_6 [13] series.

2 Computational details

The non-relativistic electronic structure calculations were carried out using the fully charge- and spin-self-consistent Korringa-Kohn-Rostoker (KKR) method [21,22]. In the KKR method we have used, both core states and valence states are calculated self-consistently. The crystal potential of muffin-tin form was constructed within the local spin density framework using the exchange-correlation term of von Barth-Hedin [23]. The self-consistency cycles were repeated for each compound until the difference between the input and output potentials was of the order of 1 mRy.

The low-temperature experimental values of the lattice parameters and the atomic coordinates deduced from the previous neutron diffraction refinements were used. For RFe_6Ge_6, an optimal filling factor of the Wigner-Seitz cell (≈62%) was obtained using non-overlapping muffin-tin spheres with radii close to 2.80 a.u., 2.55 a.u. and 2.35 a.u. for R, Fe and Ge atoms, respectively. For FeGe, the muffin-tin radii were 2.36 a.u. for Fe and 2.34 a.u. for Ge, leading to a filling factor of ≈56%. Note that for a given compound the Ge muffin-tin radii were chosen strictly equal for the inequivalent germanium sites.

For the final potentials, the total density of states (DOS), site-decomposed DOS as well as l-decomposed partial DOS (with $l_{max} = 2$, except when R = Lu for which it was necessary to include the $4f$ states in the band states to achieve a well-converged crystal potential) were computed on a 601 energy point mesh with a tetrahedral k-space integration technique using 192 small tetrahedra and 75 k-points in the irreducible part of the Brillouin zone as described in reference [24].

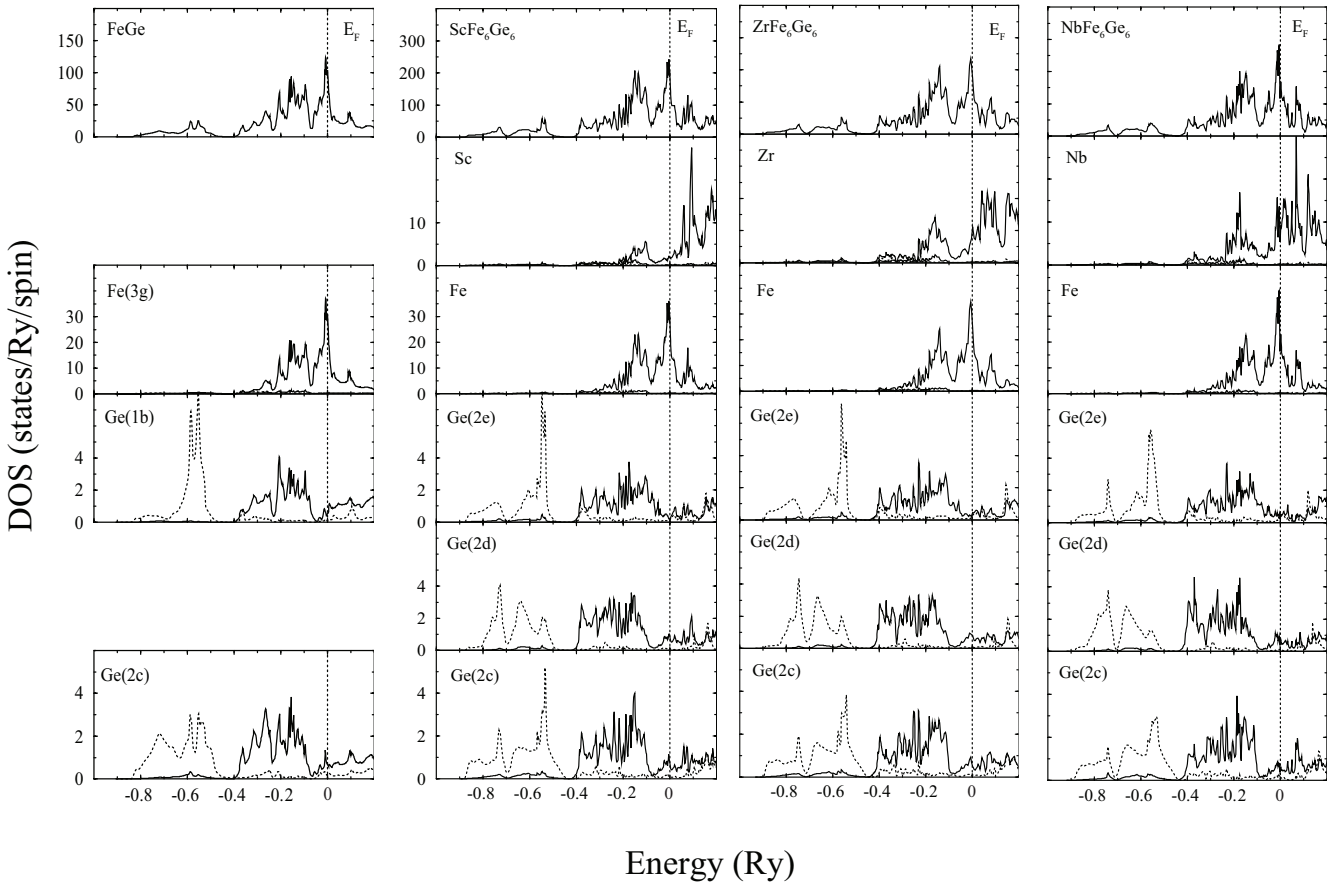

Fig. 4. KKR non-spin-polarized DOS for FeGe and some RFe_6Ge_6 compounds (R= Sc, Zr and Nb). The upper panel is the total DOS. The lower panels show l-decomposed local DOS at the various inequivalent crystallographic sites. The s, p and d contributions are plotted by dotted, solid thick and solid thin lines, respectively. For the sake of clarity the d contributions on Ge sites are not shown. The Fermi level is marked by the dotted vertical line.

Since the spin-polarized KKR calculations refer to collinear spin arrangements, a pure antiferromagnetic $(+-+-)$ structure was assumed for these compounds despite the fact that there is some experimental evidence that the magnetic moments slightly deviate from the c-axis at low temperature.

In the figures, the Fermi level (E_F) is taken as the zero of the energy scale.

3 Results and discussion

We first analyze the chemical bonding in RFe_6Ge_6 (and FeGe) based on the site-projected l-decomposed DOS arising from non-spin-polarized (NSP) calculations. Next, we discuss spin-polarized-results computed for the $(+-+-)$ antiferromagnetic ground state.

3.1 Non-spin-polarized calculations

The total DOS and the site-projected l-decomposed DOS of FeGe and some RFe_6Ge_6 compounds are shown in Figure 4. Because of the identical crystal structures and the close chemical compositions, the total DOS curves look like those previously published for RMn_6Sn_6 (R = Mg, Zr and Hf) [11]. They are characterized by low-energy states separated from other band states by a quasi-gap. These latter band states form a three clump structure whose higher energy part above E_F appears to intensify for RFe_6Ge_6 in comparison with FeGe. At first glance, we note that the electronic structure of these intermetallics results mainly from the d states of Fe and R (= Sc, Lu, Ti, Zr, Hf and Nb) mixed with the p states of Ge in the higher energy part while the lower energy-part is mostly constituted by the germanium s states.

The DOS in the Ge muffin-tin spheres are similar whatever the crystallographic site. The majority of the s states of Ge is located between ca. -0.9 Ry and -0.5 Ry and forms a two peak structure which is related to the Ge s-Ge s bonding/antibonding states. These states are also responsible, through hybridization, for the low-lying part of the d states on Fe and R atoms. The very weak s contribution on Ge atoms found at higher energy is mainly due to hybridization with the Fe d states. The germanium p states lie essentially above -0.4 Ry and, as usually found in metalloid-transition element compounds, they

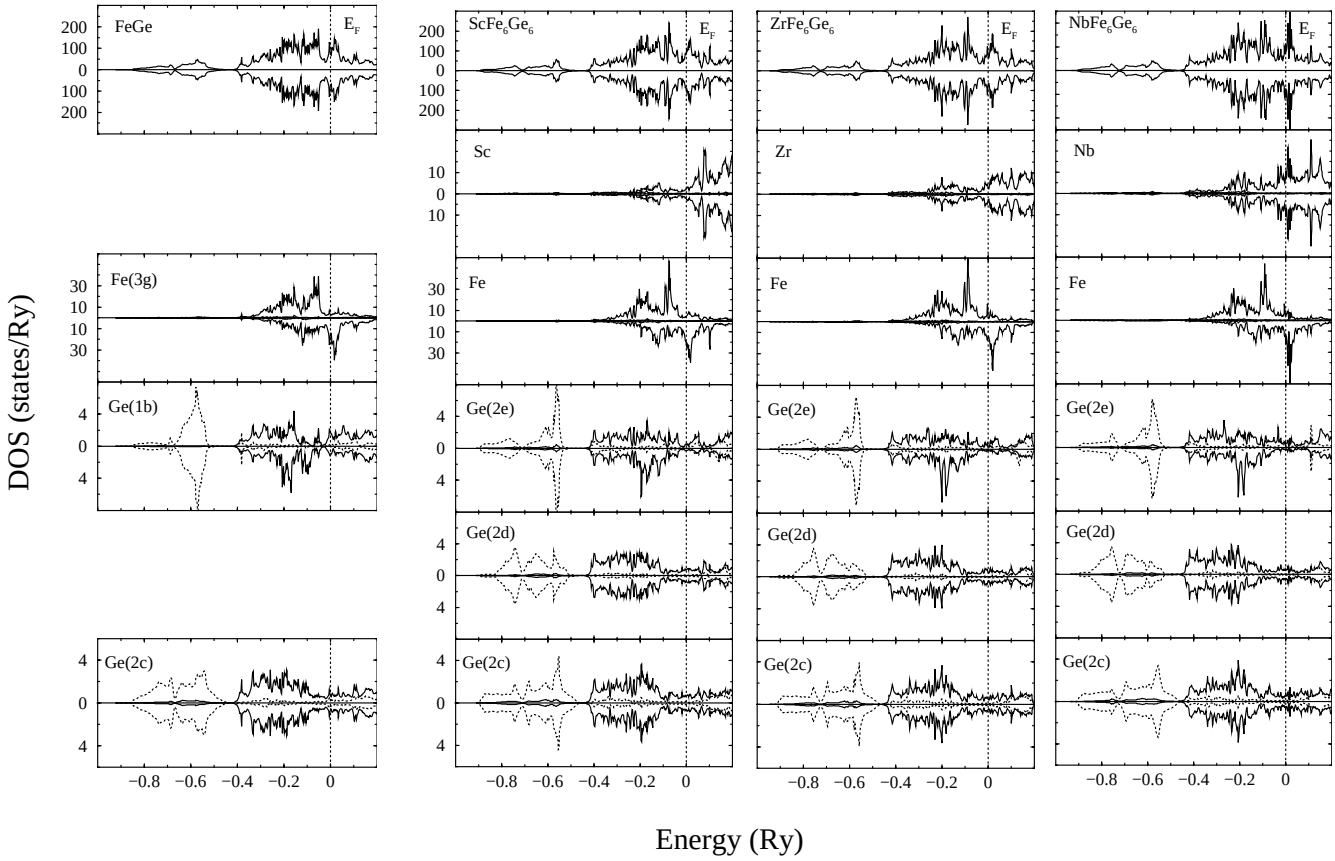

Fig. 5. KKR spin-polarized DOS for FeGe and some RFe_6Ge_6 compounds (R = Sc, Zr and Nb). The upper panel is the total DOS. The lower panels show l-decomposed local DOS at the various inequivalent crystallographic sites. The s, p and d contributions are plotted by dotted, solid thick and solid thin lines, respectively. For the sake of clarity the d contributions on Ge sites are not shown. The Fermi level is marked by the dotted vertical line.

form bonding and antibonding hybrids with Fe and R d states located at the bottom and the top of the transition metal d band respectively. Hence, the dominant part of the Ge-Fe and Ge-R bonds is due to p-d covalency.

The more intense peak in the Fe d-DOS is found at the Fermi energy and is responsible for the instability of the non-magnetic state in favor of the intratomic polarized situation (Stoner criterion). Since on other atoms the Fermi level lies in a low-density part of the site-projected DOS, we conclude that these iron d states are essentially non-bonding, at least when dealing with Fe-R and Fe-Ge bonds. On the contrary, the Fe d states found between ca. -0.4 Ry and -0.1 Ry as well as those confined in the sharp peaks above the Fermi level are strongly mixed with germanium p states and R metal states.

The R local DOS is, as expected, mainly constituted from d-symmetry states. It is characterized by two peaks of significant intensity separated by a low-density region around E_F; the two peaks are also reflected in the Fe local DOS. This gives evidence of the occurrence of a covalent interaction between the d states of Fe and the d states of the R transition element. This bond, mainly directed along the c direction, and obviously absent in FeGe, induces the shrinkage of the interplanar Fe-Fe distances upon R insertion (Fig. 2), which may appear surprising on the basis of simple steric considerations. The sharp peaks above E_F in the total DOS are thus mainly due to d-d antibonding mixed states but, since they are not completely absent in FeGe, they also involve antibonding states related to the Fe-Ge bonds.

3.2 Spin-polarized calculations

The total and l-decomposed local DOS computed for the antiferromagnetic $(+\ -\ +\ -)$ arrangement are presented in Figure 5.

3.2.1 Iron magnetic moment

The spin-polarized calculations result in strongly polarized iron local d-DOS with a (nearly) full majority-spin band (*i.e. strong ferromagnetic character*) while the Fermi level falls in the strongest peak of the minority-spin channel. It can also be seen that the Fe d-DOS does not simply arise from a rigid band shift of its non-spin-polarized counterpart.

Table 1. Calculated (m_{KKR}) and low temperature* experimental (m_{expt}) Fe magnetic moments in units of Bohr magnetons (μ_B) at the Fe site of FeGe and RFe_6Ge_6. The experimental values are taken from references [3,6,9].

	FeGe	$ScFe_6Ge_6$	$LuFe_6Ge_6$	$TiFe_6Ge_6$	$ZrFe_6Ge_6$	$HfFe_6Ge_6$	$NbFe_6Ge_6$
m_{KKR}	1.28	1.31	1.36	1.48	1.56	1.38	1.64
m_{expt}	1.60	1.52	1.45	1.68	1.96	1.90	2.05

* for R= Lu, only room temperature data are available.

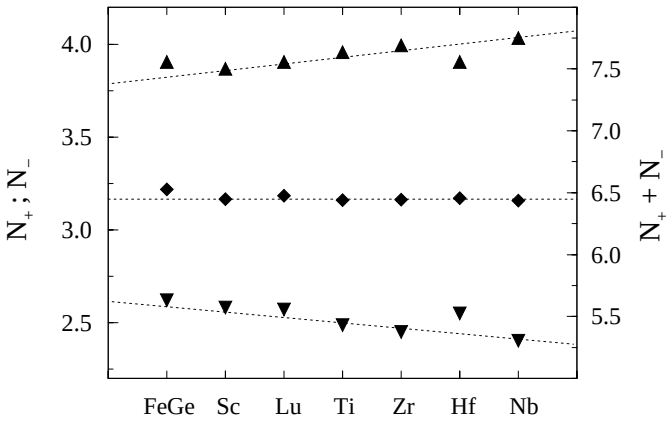

Fig. 6. Number of majority-spin (triangle up, left scale), minority-spin (triangle down, left scale) and both spin direction (diamond, right scale) *d*-symmetry electrons within the Fe muffin-tin sphere in FeGe and RFe_6Ge_6. The dotted lines are guides for the eye.

The calculated iron magnetic moments mainly arise from *d* polarization; *s* and *p* states add only a small positive contribution. The total values computed for the various compounds studied are gathered in Table 1 and compared with low temperature neutron data when available. The theoretical results reproduce well the increase of the iron magnetic moment with the R valencies experimentally observed. There is however a systematic and significant underevaluation (0.2 μ_B–0.4 μ_B) of the magnitude of the iron moment. We postpone the discussion about the possible origin of this discrepancy and first focus on the rise in the Fe moment upon increasing the R valency.

It can be seen, upon inspecting the spin-polarized local Fe DOS of FeGe or $ScFe_6Ge_6$, that adding supplementary electrons in a simple rigid band model would lead to a decrease of the Fe moment, since the minority-spin states largely dominate at the Fermi level. As shown in Figure 6, the evolution of the iron magnetic moment is due to a redistribution of the *d*-symmetry electrons within the majority-spin and minority-spin channels, the total number of *d*-symmetry electrons inside the Fe muffin-tin spheres remaining almost constant (≈6.45 electrons/at.) throughout the RFe_6Ge_6 series (R = Sc, Lu, Ti, Zr, Hf and Nb). This spin redistribution arises through a spectral weight shift below (above) the Fermi energy for the majority (minority) spin states due to spin-dependent changes in the covalent R *nd*-Fe *d* bond as we move along the RFe_6Ge_6 series.

To illustrate the underlying physics we use, similar to Williams *et al.* [14], a simple diatomic model which differentiates the two spin directions. Equivalent but more quantitative arguments were used by Brooks *et al.* [16]. The non-spin-polarized version is sketched in Figure 7a. The 3*d* Fe atomic energy levels (which approximately correspond to the center of gravity of the local density of states [25]) lie deeper in energy than the *nd* R atomic energy level since the R elements are found earlier in the transition period. Hence, the resulting bonding (antibonding) hybrids concentrate more charge on the Fe (R) atom than on the R (Fe) atom. The bonding/antibonding hybrids have been clearly identified in the KKR non-spin polarized R local DOS between ca. −0.1 and −0.2 Ry and between ca. 0.0 and 0.1 Ry, respectively (see Sect. 3.1).

This analysis also allows explaining the small "anomalies" observed for the compounds involving a 5*d* element (R = Lu and Hf). As outlined in the introduction, these compounds present ordering temperatures, iron magnetic moments and iron hyperfine fields (see Sect. 3.2.2) lower than those of the RFe_6Ge_6 compounds involving an isovalent 3*d* or 4*d* R atom. This is more perceptible when dealing with ordering temperature and hyperfine field since these two quantities are more accurately determined than the Fe moment derived from Rietveld-type powder neutron diffraction refinements. As explained by Brooks [17], the contraction of the 4*f* shell in the lanthanide series and the resulting increase in the shielding of the 5*d* states from the nucleus raises their energy (subsequently reducing the 5*d* occupation in the solid). The mixing between Fe 3*d* states and the R (= Lu and Hf) *d* states is therefore reduced in comparison with that for R = Sc and R = Ti or Zr, respectively, leading thus to a lower Fe moment.

We now switch to the possible origin of the systematic underestimation of the calculated Fe moment. Our KKR computations are non-relativistic and use the muffin-tin form of the potential. Hence, the possible anisotropy of the spin density cannot be accounted for while the (usually small) orbital moment is not evaluated. As mentioned in the introduction, the anisotropic contributions to the total Fe hyperfine field experimentally observed [4,6] clearly attest that these two effects are present on the Fe site of RFe_6Ge_6. Thus, the underevaluation of the Fe moment can likely be attributed to a non-spherical spin density and/or a not so small orbital moment. This assumption is corroborated by the close similarities in both the crystal and electronic (see *e.g.* Fig. 4 of Ref. [27]) structures of RFe_6Ge_6 and YCo_5. It is well-known from both theoretical [27–29] and experimental [26] works that Co atoms in YCo_5

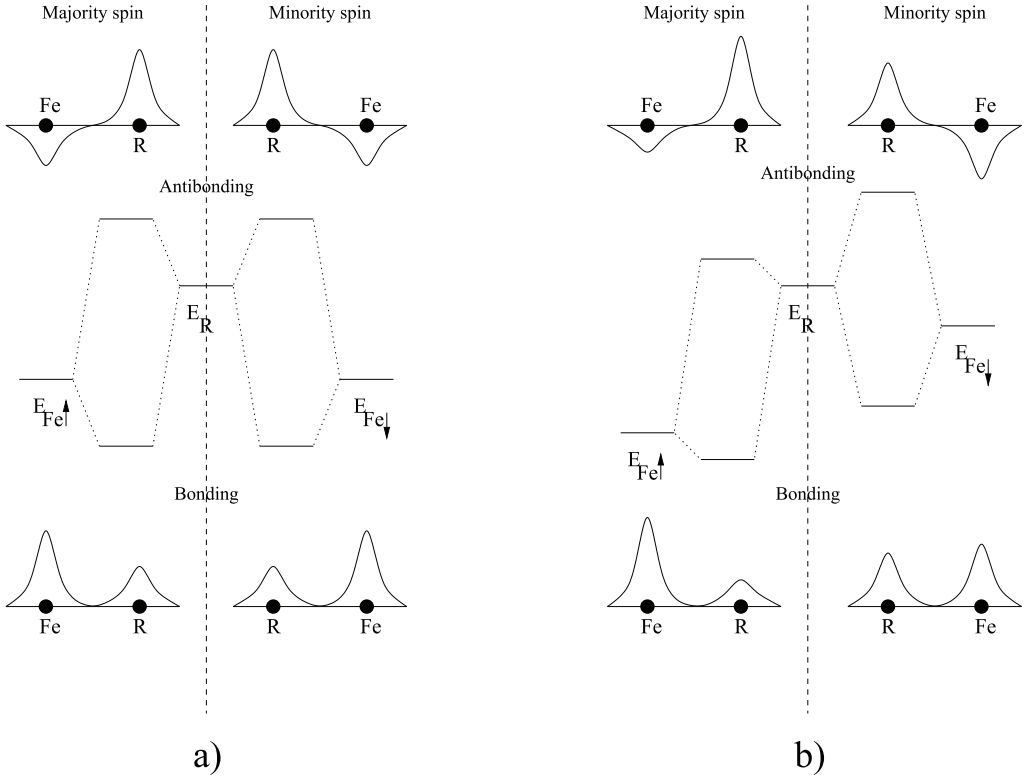

Fig. 7. Schematic drawing of the energetic levels and wave functions for the covalent R-Fe bond; a) non-spin-polarized case, b) spin-polarized case.

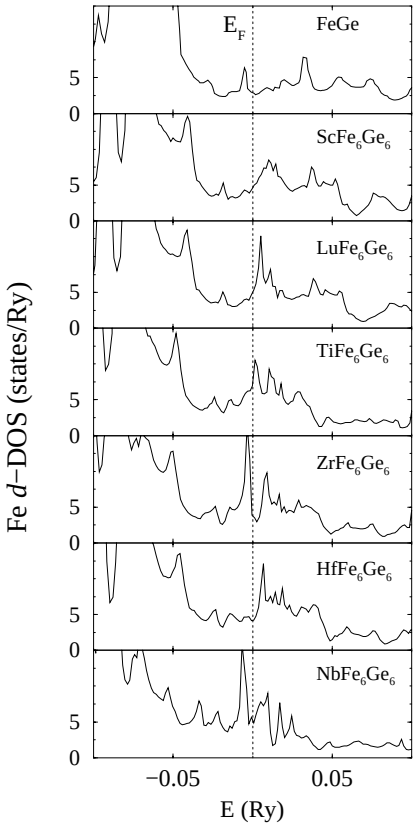

Fig. 8. Local majority-spin Fe d-DOS in the vicinity of the Fermi level for FeGe and RFe_6Ge_6.

carry one of the highest orbital moments (0.2 μ_B–0.4 μ_B) ever observed among itinerant systems (a high asphericity in the spin density on Co(2c) has also experimentally been reported). When spin-only calculations are carried out, the calculated moments are too low in comparison with the experimental values ($m_{\mathrm{Co}(2c)}$ = 1.77 μ_B and $m_{\mathrm{Co}(3g)}$ = 1.72 μ_B). For instance, our calculations lead to magnetic moments of $m_{\mathrm{Co}(2c)}$ = 1.31 μ_B and $m_{\mathrm{Co}(3g)}$= 1.37 μ_B, in good agreement with other spin-only calculations [27–30]. When spin-orbit coupling was considered, the gap between experimental and theoretical values was considerably reduced without significantly altering the computed spin moment [27,28].

3.2.2 Iron hyperfine field

The Fermi contact term to the Fe hyperfine field has been evaluated from the computed spin-dependent charge density at the nucleus using the general formula [20]:

$$H_{Fermi} = \frac{8}{3}\pi\mu_B[\rho_\uparrow(0) - \rho_\downarrow(0)]. \quad (1)$$

The total theoretical contact hyperfine field (H_{tot}) is decomposed into the valence (H_{val}) and core (H_{core}) contributions in Table 2 and compared with low temperature ^{57}Fe Mössbauer data (H_{expt}) from references [4,6]. The increase of the Fe hyperfine field upon increasing the R valency is well reproduced by the KKR results but, again, the theoretical values are too low.

Table 2. Calculated total (H_{tot}), core (H_{core}) and valence (H_{val}) hyperfine fields at the Fe nucleus of FeGe and RFe_6Ge_6 as well as low temperature experimental values (H_{expt}) taken as negative. The H'_{calc} values correspond to the total calculated hyperfine fields corrected, following Coehoorn [33], from the LDA shortcoming in evaluating the core polarization (*i.e.* -4.2 T per unit of $3d$ spin computed magnetic moment), while the H''_{calc} values were deduced from the latter by adding a constant positive orbital hyperfine field of 4.2 T, that is considering a constant orbital Fe moment of 0.1 μ_B according to Coehoorn's assumption (see text for details). All data are given in units of T. The experimental values are taken from references [4,6,8].

	FeGe	$ScFe_6Ge_6$	$LuFe_6Ge_6$	$TiFe_6Ge_6$	$ZrFe_6Ge_6$	$HfFe_6Ge_6$	$NbFe_6Ge_6$
H_{core}	-12.6	-12.9	-13.4	-14.6	-15.4	-13.6	-16.2
H_{val}	$+2.6$	$+1.8$	$+2.5$	$+3.2$	$+3.3$	$+3.0$	$+3.6$
H_{tot}	-10.0	-11.1	-11.1	-11.4	-12.1	-10.6	-12.6
H_{expt}	-15.7	-16.3	-16.1	-20.6	-21.2	-19.8	-24.0
H'_{calc}	-15.3	-16.5	-16.7	-17.4	-18.6	-16.3	-19.4
H''_{calc}	-11.1	-12.3	-12.5	-13.2	-14.2	-12.1	-15.2

Table 3. Computed Fermi contact hyperfine field values (in units of T) at the Ge(2e) nucleus of RFe_6Ge_6 [Ge(1b) nucleus in FeGe]. The sign is given with respect to the magnetic moment of the first Fe neighbors.

	FeGe	$ScFe_6Ge_6$	$LuFe_6Ge_6$	$TiFe_6Ge_6$	$ZrFe_6Ge_6$	$HfFe_6Ge_6$	$NbFe_6Ge_6$
H_{Ge}	-1.8	$+11.1$	$+11.5$	$+16.7$	$+15.9$	$+14.4$	$+18.8$

As expected, only the core hyperfine field scales with the local Fe moment and our calculations lead to the usual ratio of approximately -10 T/μ_B provided by LDA calculations for a $3d$ element [20,31]. It is also well-known that calculations performed in the local density approximation systematically underestimate the core polarization by the on site $3d$ spins [20,31–33]. According to Coehoorn [33], this error amounts to about -4.2 T per unit of $3d$ spin magnetic moment (in μ_B).

This explains why the quantitative discrepancy between computed and experimental values is worse than that found for the iron moments. The gap between theoretical and experimental values is indeed considerably reduced if the ratio proposed by Coehoorn is applied to our calculated $3d$ Fe moments to correct the calculated hyperfine field values (H'_{calc}). However, if now a positive orbital contribution is added, whose proportionality factor with orbital Fe moment is 42 T/μ_B following Coehoorn [33], a substantial difference still persists (H''_{calc}, assuming a constant orbital Fe moment of 0.1 μ_B). This analysis suggests the occurrence of a non-negligible negative contribution (say a few tesla) of dipolar origin to the total Fe hyperfine field in RFe_6Ge_6.

The valence hyperfine field scales only with the local s moment [20,31]. As a result of the small positive s moment, and contrary to the core contribution, the valence contribution is weakly positive. It is found to slightly increase upon increasing the R valency. As largely detailed in previous papers [20,31], H_{val} is built up from a positive on-site contribution due to the attractive exchange interaction with the local $3d$ moment and a negative *transferred* part arising from hybridization with the polarized d states of neighboring Fe atoms. In RFe_6Ge_6, the positive on-site contribution dominates similarly to what was computed for Fe_2P [34] or YFe_6Sn_6 [13]. Therefore, the slight increases of the valence hyperfine field observed upon increasing the R valency in the RFe_6Ge_6 series is simply the consequence of the increase of the $3d$ Fe moment.

3.2.3 Germanium hyperfine field

By contrast with the Fe hyperfine field, the Ge hyperfine field arises exclusively from valence electrons. As described by Kanamori *et al.* [18,19] in the case of *sp* impurities in ferromagnetic hosts, the spin-dependent hybridization between the self-polarized transition element $3d$ states and the impurity s states leads to low energy bonding states which show a preferential occupation for the minority-spin states at the *sp* element site, while the reverse is true for the higher energy antibonding states. Such a mechanism is directly transposable to the case of ordered compounds [11]. The Fermi contact *transferred* hyperfine field more or less scales with this induced s moment [20,31]. The similarly induced p (and d) polarization may lead to dipolar and orbital contributions to the total hyperfine field which are generally weaker than the dominant Fermi contact contribution.

Due to the $(+\ -\ +\ -)$ antiferromagnetic RFe_6Ge_6 ground state (see Fig. 1), only the Ge(2e) [Ge(1b) in FeGe] site presents an imbalance in its spin population. The computed Fermi contact hyperfine fields are indicated in Table 3. A tendency towards an increasingly positive Ge hyperfine field upon increasing the R valency is predicted: in FeGe the *transferred* hyperfine field at the Ge nucleus is weakly negative while it reaches its maximum positive

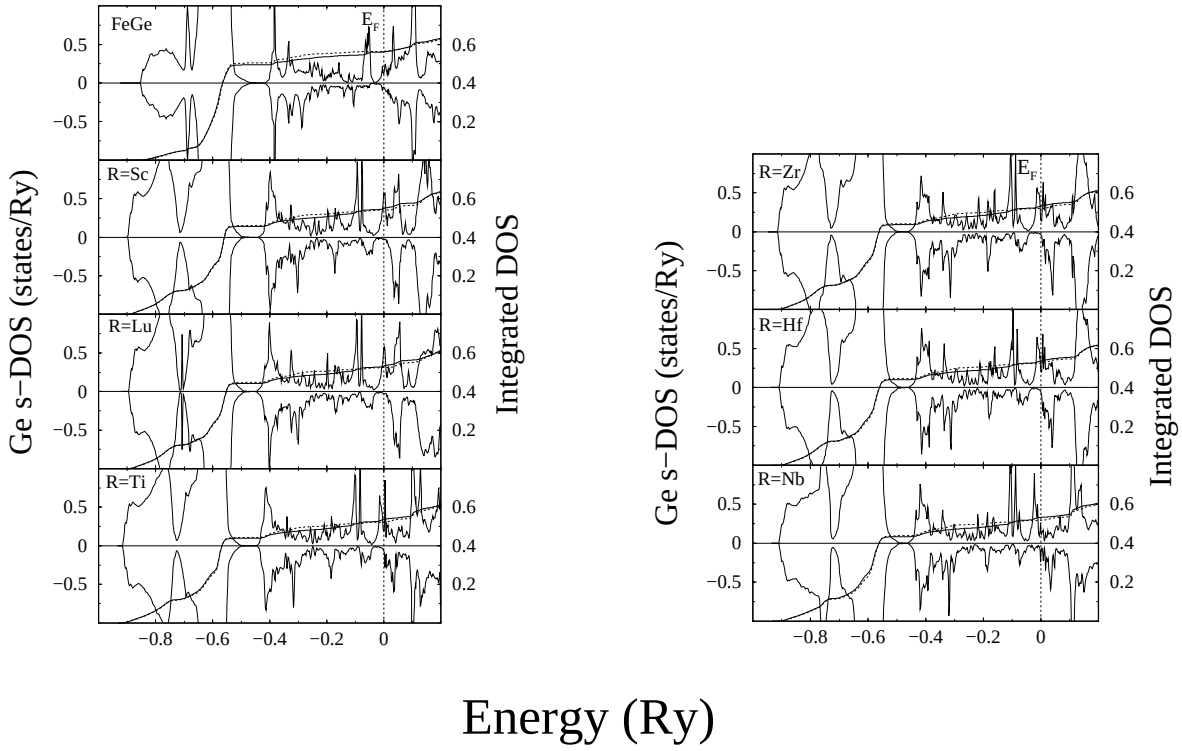

Fig. 9. Ge(1b) *s*-DOS and Ge(2e) *s*-DOS (left scale) in FeGe and RFe_6Ge_6, respectively, as well as the corresponding spin-resolved integrated DOS (right scale). Solid and dotted lines correspond to spin-up and spin-down electrons, respectively. The Fermi level is marked by the dotted vertical line.

value in $NbFe_6Ge_6$. As observed in Figure 9, where spin-dependent integrated *s*-DOS curves are superimposed on the corresponding DOS, this evolution is related to the progressive filling of a peak of antibonding character in the local Ge *s*-DOS for the majority-spin direction. We conclude that the small peaks in the majority-spin total DOS crossing the Fermi energy as we move across the series involve antibonding mixed states arising from both the Fe 3*d*-R *nd* and the Ge *sp*-Fe 3*d* bonds.

This theoretically forecasted trend should be checked by ^{73}Ge NMR experiments [35]. A quantitative agreement as close as what we previously obtained for the strongly negative Sn hyperfine fields in RMn_6Sn_6 (R = Mg, Zr and Hf) [11] is however not necessarily expected. Change from huge negative Sn hyperfine fields in RMn_6Sn_6 to positive Ge hyperfine fields in RFe_6Ge_6 can be understood on the basis of a rigid band approach: in the Mn-based compounds only the bonding *s*-*d* hybrids are occupied while in iron systems the supplementary valence electrons partly populate the antibonding states.

4 Summary

The electronic structure of FeGe and the derived RFe_6Ge_6 compounds (R = Sc, Lu, Ti, Zr, Hf and Nb) has been studied using the non-relativistic muffin-tin KKR method within the LDA framework.

When an early R transition element is inserted in the layered CoSn-type FeGe host framework, it forms a covalent *d*-*d* bond with the iron states which causes the shrinkage of the Fe-Fe interplanar distance. The experimentally observed increase in both the iron moments and iron hyperfine fields with the R valency has been explained in terms of spin-dependent changes in this *d*-*d* interaction as we move across the RFe_6Ge_6 series. The relatively poor quantitative agreement between the computed and experimental values for these two parameters has been tentatively interpreted as being due to the occurrence of a significant anisotropy in the spin density as well as a non-negligible orbital moment at the iron site. This point could be clarified, for instance, by polarized neutron experiments and by fully-relativistic full-potential calculations. Finally, the KKR results also predict a strong variation of the Ge(2e) *transferred* hyperfine field with the R valency.

References

1. R.R. Olenitch, L.G. Aksel'rud, Ya.P. Yarmoliuk, Dopov. Akad. Nauk. Ukr RSR Ser. A **2**, 84 (1981)
2. G. Venturini, R. Welter, B. Malaman, J. Alloys Compd. **185**, 99 (1992)
3. P. Schobinger-Papamantellos, K.H.J. Buschow, F.R. de Boer, C. Ritter, O. Isnard, F. Fauth, J. Alloys Compd. **267**, 59 (1998)

4. T. Mazet, B. Malaman, J. Phys. Cond. Matt. **12**, 1085 (2000)
5. P. Villars, L.D. Calvert, *Pearson's Handbook of Crystallographic Data for Intermetallic Phases* (American Society for Metals, Metals Park, OH, 1985)
6. T. Mazet, O. Isnard, B. Malaman, Solid State Commun. **114**, 91 (2000)
7. T. Mazet, B. Malaman, J. Alloys Compd. **325**, 67 (2001)
8. L. Häggström, T. Ericsson, R. Wäppling, E. Karlsson, Physica Scripta **55**, 11 (1974)
9. J.B. Forsyth, C. Wilkinson, P. Gardner, J. Phys. F **8**, 2195 (1978)
10. J. Bernhard, B. Lebech, O. Beckman, J. Phys. F **14**, 2379 (1984)
11. T. Mazet, J. Tobola, G. Venturini, B. Malaman, Phys. Rev. B **65**, 104406 (2002)
12. M.T. Kelemen, M.S.S. Brooks, E. Dormann, J. Phys. Cond. Matt. **13**, 657 (2001)
13. X. Rao, J. Cullen, V. Skumryev, J.M.D. Coey, J. Appl. Phys. **83**, 6983 (1998)
14. A.R. Williams, R. Zeller, V.L. Moruzzi, C.D. Gellat, J. Kubler, J. Appl. Phys. **52**, 2067 (1981)
15. K. Terakura, J. Phys. F **9**, 2469 (1979)
16. M.S.S. Brooks, O. Eriksson, B. Johansson, J. Phys. Cond. Matt. **1**, 5861 (1989)
17. M.S.S. Brooks, L. Nordström, B. Johansson, J. Phys. Cond. Matt. **3**, 2357 (1991)
18. J. Kanamori, H. Katayama-Yoshida, K. Terakura, Hyperfine Interact. **8**, 573 (1981)
19. J. Kanamori, H. Katayama-Yoshida, K. Terakura, Hyperfine Interact. **9**, 363 (1981)
20. H. Akai, M. Akai, S. Blügel, B. Drittler, H. Ebert, K. Terakura, R. Zeller, P.H. Dederichs, Suppl. Prog. Theor. Phys. **101**, 11 (1990) and references therein
21. A. Bansil, S. Kaprzyk, P.E. Mijnarends, J. Tobola, Phys. Rev. B **60**, 13396 (1999) and references therein
22. S. Kaprzyk, Acta Phys. Pol. A **91**, 135 (1997)
23. U. von Barth, L. Hedin, J. Phys. C **5**, 1629 (1972)
24. S. Kaprzyk, P.E. Mijnarends, J. Phys. C **19**, 1283 (1986)
25. D.G. Pettifor, *Solid State Physics,* Vol. 40, edited by H. Ehrenreich, D. Turnbull (Academic Press, London, 1987), p. 43
26. J. Schweizer, F. Tasset, J. Phys. F **10**, 2799 (1980)
27. L. Nordström, O. Eriksson, M.S.S. Brooks, B. Johansson, Phys. Rev. B **41**, 9111 (1990)
28. G.H.O. Daalderop, P.J. Kelly, M.F.H. Schuurmans, Phys. Rev. B **44**, 12054 (1991)
29. L. Nordström, M.S.S. Brooks, B. Johansson, J. Magn. Magn. Mater. **104-107**, 1942 (1992)
30. I. Kitagawa, K. Terao, M. Aoki, H. Yamada, J. Phys. Cond. Matt. **9**, 231 (1997)
31. S. Blügel, H. Akai, R. Zeller, P.H. Dederichs, Phys. Rev. B **35**, 3271 (1987)
32. H. Ebert, H. Akai, Hyperfine Interact. **78**, 361 (1993)
33. R. Coehoorn, J. Magn. Magn. Mater. **159**, 55 (1996)
34. O. Eriksson, A. Svane, J. Phys. Cond. Matt. **1**, 1589 (1989)
35. P. Rösch, M.T. Kelemen, B. Pilawa, E. Dormann, K.H.J. Bushow, J. Magn. Magn. Mater. **164**, 175 (1996)